JOURNAL OF COMPUTATIONAL PHYSICS 98, 163–173 (1992)

Application of Bubnov–Galerkin Formulation to Orthogonal Grid Generation

ALEJANDRO ALLIEVI AND SANDER M. CALISAL

Department of Mechanical Engineering, University of British Columbia, Vancouver, Canada V6T 1W5

Received April 6, 1990; accepted January 31, 1991

A Bubnov–Galerkin formulation is used to solve an elliptic grid generation system by using linear and quadratic isoparametric elements. Good orthogonality characteristics are obtained for symmetric and non-symmetric physical domains using both complete boundary correspondence or a combination of Dirichlet and Neuman boundary conditions. The method exhibits excellent stability and requires a low number of iterations to attain convergence. Results are compared with those presented in (E. D. Chikliwala and Y. C. Yortsos, *J. Comput. Phys.* **57**, 391, 1985). © 1992 Academic Press, Inc.

I. INTRODUCTION

It has been pointed out by several researchers that, regardless of the numerical method used for the solution of partial differential equations, the accuracy obtained is closely related to the "quality" of the generated mesh. One component of this quality is the orthogonality characteristics. A thorough description of different procedures for the estimation of orthogonal grids can be found in [3]. Elliptic systems can provide orthogonal grids of good accuracy. One system that is particularly attractive is that developed in [4]. It requires the calculation of only one line control function for both generating equations in two dimensions. It is also relatively simple to implement using a Bubnov–Galerkin procedure.

This paper is an attempt to use a Bubnov–Galerkin formulation to solve the weak constraint method for the construction of boundary-fitted orthogonal curvilinear coordinates developed in [4]. Numerical computations are carried out on a particular domain encounter in immiscible displacement processes [6]. This domain has been used here in order to facilitate comparison and bècause the wave-like shape of one of its boundaries is commonly encountered in the author's field of marine/ship hydrodynamics. Although orthogonal coordinates are not required when applying the finite element method, it has long been realized [12] that the error in the element depends on the angle formed by the adjacent sides. Therefore, the lowest departure of this angle from orthogonality is likely to give improved results.

Elliptic Generating System

The generating system used in this work is

$$\frac{\partial}{\partial \varepsilon}\left[f\frac{\partial x}{\partial \varepsilon}\right]+\frac{\partial}{\partial \varrho}\left[\frac{1}{f}\frac{\partial x}{\partial \varrho}\right]=0$$
$$\frac{\partial}{\partial \varepsilon}\left[f\frac{\partial y}{\partial \varepsilon}\right]+\frac{\partial}{\partial \varrho}\left[\frac{1}{f}\frac{\partial y}{\partial \varrho}\right]=0, \tag{1.1}$$

where

$$f^2 = g_{22}/g_{11} \tag{1.2}$$

$$g_{11} = x_{,\varepsilon}^2 + y_{,\varepsilon}^2$$
$$g_{22} = x_{,\varrho}^2 + y_{,\varrho}^2 \tag{1.3}$$

with g_{11} and g_{22} being the elements of the main diagonal of the *covariant* metric tensor. Equations (1.1) define an elliptic system developed in [4] and applied to a specific geometry using a finite difference discretization in [6]. In the following developments a Bubnov–Galerkin formulation is presented and applied to solve system (1.1). Numerical results are obtained and compared with those reported in [6] for exactly the same geometries used in this reference.

II. BUBNOV–GALERKIN PROCEDURE

In this section, we develop the method to solve the field equation (1.1), valid in the whole transformed domain Ω surrounded by the contour Γ, as discrete points selectively specified. The method used, a Bubnov–Galerkin procedure, is one of the so-called *methods of weighted residuals*. The basic idea of these methods [1] is to obtain a solution of a differential equation

$$-A\phi - f = 0 \qquad \text{in } \Omega, \tag{2.1}$$

subject to boundary conditions on the contour Γ by introducing an approximate function in the form

$$\hat{\Phi} = \sum_{i=1}^{n} C_j \Phi_j, \tag{2.2}$$

0021-9991/92 $3.00

where the C_j are constants and the Φ_j are linearly independent functions chosen so that global boundary conditions may or may not be satisfied. Since (2.2) is an approximate function we note that, when substituted into (2.1), it will not satisfy the governing differential equation. Then we write

$$-A\hat{\Phi} - f = R, \tag{2.3}$$

where R is an error quantity or *residual*. Let us now introduce a set of weighting functions w_i ($i = 1, 2, ..., n$) and construct the inner product (R, w_i). Next, set the inner product equal to zero

$$(R, w_i) = 0, \tag{2.4}$$

which is equivalent to forcing the residual to be zero in an average sense. The choice of the weighting functions w_i determines the weighted residual method. In a Bubnov–Galerkin procedure [7, 8] the weighting functions are made equal to the trial (base, shape) functions Φ_j. In effect, this is equivalent to an orthogonal projection of the residual R onto each of a set of linearly independent functions Φ_i as implied by (2.4). In order for $\hat{\Phi}$ to be the exact solution of the given differential equation, it is necessary that R is identical to zero. This requirement, if R is considered continuous, is equivalent to requiring the orthogonality of the expression for R to all the functions Φ_i, $i = 1, 2, ..., n$ [7, 8]. However, having at our disposal only a finite number n of constants $C_1, C_2, ..., C_n$, we can only satisfy n conditions of orthogonality. Based on these considerations we write

$$(R, w_i) = (R, \Phi_i) = \int_\Omega R\Phi_i \, d\Omega = \int_\Omega \left[A\left(\sum_{j=1}^{n} C_j \Phi_j + f \right) \right] \Phi_i \, d\Omega = 0 \tag{2.5}$$

which serves for the determination of the coefficients C_j. On finding the C_j from this system of equations and substituting them into the expression for $\hat{\Phi}$ gives the required approximate solution. However, if we set the C_j to be our unknown variables, the problem is solved when solving (2.5). To illustrate this concept, let us look at one of the equations defining the elliptic system (1.2). For the x-coordinate we have

$$\frac{\partial}{\partial \varepsilon}\left[f \frac{\partial x}{\partial \varepsilon} \right] + \frac{\partial}{\partial \varrho}\left[\frac{1}{f} \frac{\partial x}{\partial \varrho} \right] = 0.$$

Let the approximate function $\hat{x}$ for the variable x be given by an expression like (2.2) as

$$\hat{x} = \sum_{j=1}^{n} C_j \Phi_j, \tag{2.6}$$

then the residual for (1.1) becomes

$$\frac{\partial}{\partial \varepsilon}\left[f \frac{\partial \hat{x}}{\partial \varepsilon} \right] + \frac{\partial}{\partial \varrho}\left[\frac{1}{f} \frac{\partial \hat{x}}{\partial \varrho} \right] = R \tag{2.7}$$

and the inner product (R, w_i) from (2.5) gives

$$(R, \Phi_i) = \iint R\Phi_i \, d\varepsilon \, d\varrho = \iint \left\{ \frac{\partial}{\partial \varepsilon}\left[f \frac{\partial \hat{x}}{\partial \varepsilon} \right] + \frac{\partial}{\partial \varrho}\left[\frac{1}{f} \frac{\partial \hat{x}}{\partial \varrho} \right] \Phi_i \right\} d\varepsilon \, d\varrho = 0. \tag{2.8}$$

The relationship connecting the surface integral for the flux of a vector field with the volume integral of its divergence is known as the Green–Gauss theorem and is expressed [9]

$$\int_\Omega \alpha V_{i,i} \, d\Omega = \int_\Gamma \alpha V_i n_i \, d\Gamma - \int_\Omega V_i \alpha_{,i} \, d\Omega, \tag{2.9}$$

where the comma denotes derivatives. Applying (2.9) to (2.8) in a two-dimensional domain gives

$$\iint \left\{ f \frac{\partial \hat{x}}{\partial \varepsilon} \frac{\partial \Phi_i}{\partial \varepsilon} + \frac{1}{f} \frac{\partial \hat{x}}{\partial \varrho} \frac{\partial \Phi_i}{\partial \varrho} \right\} d\varepsilon \, d\varrho = \int_\Gamma \Phi_i \left\{ \left(f \frac{\partial \hat{x}}{\partial \varepsilon} \right) \mathbf{n}_\varepsilon + \left(\frac{1}{f} \frac{\partial \hat{x}}{\partial \varrho} \right) \mathbf{n}_\varrho \right\} d\Gamma, \tag{2.10}$$

and, similarly for the y-coordinate, we write

$$\iint \left\{ f \frac{\partial \hat{y}}{\partial \varepsilon} \frac{\partial \Phi_i}{\partial \varepsilon} + \frac{1}{f} \frac{\partial \hat{y}}{\partial \varrho} \frac{\partial \Phi_i}{\partial \varrho} \right\} d\varepsilon \, d\varrho = \int_\Gamma \Phi_i \left\{ \left(f \frac{\partial \hat{y}}{\partial \varepsilon} \right) \mathbf{n}_\varepsilon + \left(\frac{1}{f} \frac{\partial \hat{y}}{\partial \varrho} \right) \mathbf{n}_\varrho \right\} d\Gamma, \tag{2.11}$$

where

$$\hat{y} = \sum_{j=1}^{n} D_j \Phi_j.$$

So far we have stated our problem in a global sense, i.e., for the entire physical domain Ω. The essential principle of the *finite element method* is that a continuum is divided into elements of suitable shape. The differential equations to be solved, (2.10) and (2.11), are written as a combination of appropriately selected interpolation functions. Since these functions can rarely be found for a whole domain, we find them for each element separately and satisfy certain continuity conditions at the elements' common boundaries. These shape functions are written at suitably chosen points on the element, i.e., *the nodes of the element*. Thus (2.10) and

(2.11) can be considered our elemental equations with the interpolation functions written for each individual element. The equations written for each element are collected together to form a global system of algebraic equations. After introducing boundary conditions, nodal values of the variable can be calculated. We now proceed to discuss the type of elements to be used in this work.

III. THE ISOPARAMETRIC ELEMENT

Details on the origins, applications, and theoretical development that follow can be found in [10]. The name isoparametric derives from the fact that the same parametric functions Φ_i that describe the geometry of the element may be used for interpolating spatial variations of the unknown field variable on the element.

Consider now a square element. The origin of the isoparametric coordinates (ξ, η) whose values range from 0 to ± 1 are established at the center of the element. The reference coordinate system is here (ε, ϱ) and is related to (ξ, η) for two-dimensional quadratic elements as

$$\begin{aligned}\varepsilon &= a_1 + a_2\xi + a_3\eta + a_4\xi^2 + a_5\xi\eta + a_6\eta^2 + a_7\xi^2\eta + a_8\xi\eta^2\\ \varrho &= b_1 + b_2\xi + b_3\eta + b_4\xi^2 + b_5\xi\eta + b_6\eta^2 + b_7\xi^2\eta + b_8\xi\eta^2.\end{aligned} \tag{3.1}$$

We can now write (3.1) in terms of the corner and mid-side nodal values,

$$\begin{aligned}\varepsilon_i &= a_1 + a_2\xi_i + a_3\eta_i + a_4\xi_i^2 + a_5\xi_i\eta_i + a_6\eta_i^2\\ &\quad + a_7\xi_i^2\eta_i + a_8\xi_i\eta_i^2\\ \varrho_i &= b_1 + b_2\xi_i + b_3\eta_i + b_4\xi_i^2 + b_5\xi_i\eta_i + b_6\eta_i^2\\ &\quad + b_7\xi_i^2\eta_i + b_8\xi_i\eta_i^2\end{aligned} \tag{3.2}$$

with $i = 1, \ldots, 8$. In matrix form Eqs. (3.2) are

$$\begin{aligned}\{\varepsilon_i\} &= [C]\{a_i\}\\ \{\varrho_i\} &= [C]\{b_i\}\end{aligned} \tag{3.3}$$

or

$$\begin{aligned}\{a_i\} &= [C]^{-1}\{\varepsilon_i\}\\ \{b_i\} &= [C]^{-1}\{\varrho_i\}\end{aligned} \tag{3.4}$$

which are the polynomial coefficients in terms of the nodal coordinates of the *computational domain.* We can see that the matrix $[C]$, made up by the element's nodal coordinates in the (ξ, η) system, is the same for both $\{a_i\}$ and $\{b_i\}$. Inversion of $[C]$ in (3.4) and substitution of the coefficients into (3.1) gives

$$\begin{aligned}\varepsilon &= \sum_{i=1}^{8} \Phi_i\varepsilon_i\\ \varrho &= \sum_{i=1}^{8} \Phi_i\varrho_i,\end{aligned} \tag{3.5}$$

where [11]

$$\begin{aligned}\Phi_1 &= -\tfrac{1}{4}(1-\xi)(1-\eta)(1+\xi+\eta)\\ \Phi_2 &= -\tfrac{1}{4}(1+\xi)(1-\eta)(1-\xi+\eta)\\ \Phi_3 &= -\tfrac{1}{4}(1+\xi)(1+\eta)(1-\xi-\eta)\\ \Phi_4 &= -\tfrac{1}{4}(1-\xi)(1+\eta)(1+\xi-\eta)\\ \Phi_5 &= \tfrac{1}{2}(1-\xi^2)(1-\eta)\\ \Phi_6 &= \tfrac{1}{2}(1-\eta^2)(1+\xi)\\ \Phi_7 &= \tfrac{1}{2}(1-\xi^2)(1+\eta)\\ \Phi_8 &= \tfrac{1}{2}(1-\eta^2)(1-\xi).\end{aligned} \tag{3.6}$$

As mentioned above, the isoparametric element uses the same parametric functions to define the relationship between reference global coordinates and local parametric coordinates as to describe the variation of the given variable within the element. The unknown variables in this particular case of mesh generation are the cartesian coordinates of the physical domain. Then we write

$$\begin{aligned}\hat{x} &= \sum_{i=1}^{8} x_i\Phi_i\\ \hat{y} &= \sum_{i=1}^{8} y_i\Phi_i,\end{aligned} \tag{3.7}$$

where the Φ_i are the same parametric functions as (3.6) and x_i, y_i are the nodal values of the cartesian coordinates. These nodal parameters are then equivalent to the constants C_j in (2.2).

A similar development could be followed for the case of a linear isoparametric element. In this case, only linear terms in ξ and η are taken in (3.1). The resulting approximation for (ε, ϱ) is

$$\begin{aligned}\varepsilon &= \sum_{i=1}^{4} \varepsilon_i\Phi_i\\ \varrho &= \sum_{i=1}^{4} \varrho_i\Phi_i\end{aligned} \tag{3.8}$$

and for $(\hat{x}, \hat{y})$ is

$$\begin{aligned}\hat{x} &= \sum_{i=1}^{4} x_i\Phi_i\\ \hat{y} &= \sum_{i=1}^{4} y_i\Phi_i\end{aligned} \tag{3.9}$$

with

$$\begin{aligned}\Phi_1 &= \tfrac{1}{4}(1-\xi)(1-\eta)\\ \Phi_2 &= \tfrac{1}{4}(1+\xi)(1-\eta)\\ \Phi_3 &= \tfrac{1}{4}(1+\xi)(1+\eta)\\ \Phi_4 &= \tfrac{1}{4}(1-\xi)(1+\eta),\end{aligned} \tag{3.10}$$

where *only* the corner nodes are to be considered.

IV. FINITE ELEMENT FORMULATION

In Section II we obtained expressions which were the result of a weighted residual procedure. These expressions, (2.10) and (2.11), contained approximation functions, $\hat{x}$ and $\hat{y}$, that were to be defined on an elemental level. In Section III, those functions were defined for linear and quadratic isoparametric elements. In this section, we combine Eqs. (2.10) and (2.11) with (3.5), (3.6), and (3.7) for quadratic elements or (3.8), (3.9), and (3.10) for linear elements. The upper limit in the sumation signs will be left unspecified and understood as $n = 4$ and $n = 8$ for linear and quadratic elements, respectively. The Bubnov–Galerkin procedure for the x-coordinate gave

$$\iint \left\{ f \frac{\partial \hat{x}}{\partial \varepsilon}\frac{\partial \Phi_i}{\partial \varepsilon} + \frac{1}{f}\frac{\partial \hat{x}}{\partial \varrho}\frac{\partial \Phi_i}{\partial \varrho}\right\} d\varepsilon\, d\varrho = \int_\Gamma \Phi_i \left\{ \left(f\frac{\partial \hat{x}}{\partial \varepsilon}\right)\mathbf{n}_\varepsilon + \left(\frac{1}{f}\frac{\partial \hat{x}}{\partial \varrho}\right)\mathbf{n}_\varrho \right\} d\Gamma, \tag{2.11}$$

introducing (3.7) or (3.9) into (2.11) gives an elemental equation as

$$\iint_{\Omega_k} \sum_{j=1}^{n} x_j \left\{ f_j \frac{\partial \Phi_j}{\partial \varepsilon}\frac{\partial \Phi_i}{\partial \varepsilon} + \frac{1}{f_j}\frac{\partial \Phi_j}{\partial \varrho}\frac{\partial \Phi_i}{\partial \varrho}\right\} d\varepsilon\, d\varrho = \int_{\Gamma_l} \Phi_i \left\{ \left(f_{\Gamma_l}\frac{\partial \hat{x}}{\partial \varepsilon}\right)\mathbf{n}_\varepsilon + \left(\frac{1}{f_{\Gamma_l}}\frac{\partial \hat{x}}{\partial \varrho}\right)\mathbf{n}_\varrho \right\} d\Gamma, \tag{4.1}$$

where the subindexes k and l refer, respectively, to the element Ω_k and the boundary Γ_l in contact with the contour of the domain. Equation (4.1) contains the ε and ϱ variables, yet the interpolation functions were expressed in terms of the local (ξ, η) coordinates. Thus we require a transformation between these two domains. This transformation corresponds to the mapping of an element on the *computational domain* (ε, ϱ) to an element defined by the isoparametric coordinates. The transformed domain can, for convenience, be taken as a square with unit sides and our element equation (4.1) applied to a given element on this square.

Consider now the chain rule expressions

$$\begin{aligned}\frac{\partial \Phi_j}{\partial \xi} &= \frac{\partial \Phi_j}{\partial \varepsilon}\frac{\partial \varepsilon}{\partial \xi} + \frac{\partial \Phi_j}{\partial \varrho}\frac{\partial \varrho}{\partial \xi}\\ \frac{\partial \Phi_j}{\partial \eta} &= \frac{\partial \Phi_j}{\partial \varepsilon}\frac{\partial \varepsilon}{\partial \eta} + \frac{\partial \Phi_j}{\partial \varrho}\frac{\partial \varrho}{\partial \eta}\end{aligned} \tag{4.2}$$

or, in matrix form,

$$\begin{bmatrix} \dfrac{\partial \Phi_j}{\partial \xi} \\ \dfrac{\partial \Phi_j}{\partial \eta} \end{bmatrix} = \begin{bmatrix} \dfrac{\partial \varepsilon}{\partial \xi} & \dfrac{\partial \varrho}{\partial \xi} \\ \dfrac{\partial \varepsilon}{\partial \eta} & \dfrac{\partial \varrho}{\partial \eta} \end{bmatrix} \begin{bmatrix} \dfrac{\partial \Phi_j}{\partial \varepsilon} \\ \dfrac{\partial \Phi_j}{\partial \varrho} \end{bmatrix}.$$

Thus

$$\begin{bmatrix} \dfrac{\partial \Phi_j}{\partial \varepsilon} \\ \dfrac{\partial \Phi_j}{\partial \varrho} \end{bmatrix} = J^{-1} \begin{bmatrix} \dfrac{\partial \Phi_j}{\partial \xi} \\ \dfrac{\partial \Phi_j}{\partial \eta} \end{bmatrix} = \begin{bmatrix} \bar{J}_{11} & \bar{J}_{12} \\ \bar{J}_{21} & \bar{J}_{22} \end{bmatrix} \begin{bmatrix} \dfrac{\partial \Phi_j}{\partial \xi} \\ \dfrac{\partial \Phi_j}{\partial \eta} \end{bmatrix}, \tag{4.3}$$

where J is the Jacobian matrix given by

$$J = \begin{bmatrix} \dfrac{\partial \varepsilon}{\partial \xi} & \dfrac{\partial \varrho}{\partial \xi} \\ \dfrac{\partial \varepsilon}{\partial \eta} & \dfrac{\partial \varrho}{\partial \eta} \end{bmatrix}.$$

The integration over the domain Ω_k referred to the (ε, ϱ) coordinates must also be changed to the isoparametric coordinates. Then we have [10]

$$\iint d\varepsilon\, d\varrho = \int_{-1}^{+1}\int_{-1}^{+1} \det[J]\, d\xi\, d\eta; \tag{4.4}$$

introducing (4.3) and (4.4) into (4.1) gives

$$\begin{aligned}\int_{-1}^{+1}\int_{-1}^{+1} \sum_{j=1}^{n} x_j \Bigg\{ f_j \left[\bar{J}_{11}\frac{\partial \Phi_j}{\partial \xi} + \bar{J}_{12}\frac{\partial \Phi_j}{\partial \eta}\right]\left[\bar{J}_{11}\frac{\partial \Phi_i}{\partial \xi} + \bar{J}_{12}\frac{\partial \Phi_i}{\partial \eta}\right] \\ + \frac{1}{f_j}\left[\bar{J}_{21}\frac{\partial \Phi_j}{\partial \xi} + \bar{J}_{22}\frac{\partial \Phi_j}{\partial \eta}\right] \\ \times \left[\bar{J}_{21}\frac{\partial \Phi_i}{\partial \xi} + \bar{J}_{22}\frac{\partial \Phi_i}{\partial \eta}\right]\Bigg\} \det[J]\, d\xi\, d\eta \\ = \int_{\Gamma_l} \Phi_i \left\{ \left(f_{\Gamma_l}\frac{\partial x}{\partial \varepsilon}\right)\mathbf{n}_\varepsilon + \left(\frac{1}{f_{\Gamma_l}}\frac{\partial x}{\partial \varrho}\right)\mathbf{n}_\varrho \right\} d\Gamma_l.\end{aligned} \tag{4.5a}$$

Similarly, for the y-coordinate we have

$$\int_{-1}^{+1}\int_{-1}^{+1}\sum_{j=1}^{n} y_j \left\{ f_j \left[\bar{J}_{11}\frac{\partial \Phi_j}{\partial \xi} + \bar{J}_{12}\frac{\partial \Phi_j}{\partial \eta} \right] \left[\bar{J}_{11}\frac{\partial \Phi_i}{\partial \xi} + \bar{J}_{12}\frac{\partial \Phi_i}{\partial \eta} \right] + \frac{1}{f_j}\left[\bar{J}_{21}\frac{\partial \Phi_j}{\partial \xi} + \bar{J}_{22}\frac{\partial \Phi_j}{\partial \eta} \right] \times \left[\bar{J}_{21}\frac{\partial \Phi_i}{\partial \xi} + \bar{J}_{22}\frac{\partial \Phi_i}{\partial \eta} \right] \right\} \det[J]\, d\xi\, d\eta$$

$$= \int_{\Gamma_l} \Phi_i \left\{ \left(f_{\Gamma_l}\frac{\partial y}{\partial \varepsilon} \right) \mathbf{n}_\varepsilon + \left(\frac{1}{f_{\Gamma_l}}\frac{\partial y}{\partial \varrho} \right) \mathbf{n}_\varrho \right\} d\Gamma_l. \tag{4.5b}$$

We can see that the left-hand sides of (4.5) and (4.6) give an $n \times n$ algebraic system for each element. It should be noticed here that (4.5) will, in general, give a non-symmetric matrix. This inconvenience can be circumvented by obtaining an average value $\hat{f}_k$ for each element. The right-hand side in (4.5) contains line integrals with derivatives of the cartesian coordinates with respect to the (ε, ϱ) coordinates of the computational domain. When this integral is evaluated at any given boundary, the boundary condition is termed as *Neuman* boundary condition. When the right-hand side of (4.5) is either made equal to the x or y coordinate of the boundary and the row and column of the corresponding main diagonal element are zeroed, the boundary condition is termed *Dirichlet* boundary condition.

Equations (4.5) require the numerical estimation of surface and line integrals. This can performed using Gauss quadrature [10]. In this work 2×2 points were used for linear elements and 3×3 for quadratic ones.

V. CALCULATION OF THE SHAPE FACTOR f

The shape factor f was defined in (1.2). Then using (1.3) and (3.7) or (3.9) gives

$$g_{11} = \left(\sum_{i=1}^{n} x_i \frac{\partial \Phi_i}{\partial \varepsilon} \right)^2 + \left(\sum_{i=1}^{n} y_i \frac{\partial \Phi_i}{\partial \varepsilon} \right)^2$$
$$g_{22} = \left(\sum_{i=1}^{n} x_i \frac{\partial \Phi_i}{\partial \varrho} \right)^2 + \left(\sum_{i=1}^{n} y_i \frac{\partial \Phi_i}{\partial \varrho} \right)^2. \tag{5.1}$$

Now again we have the derivatives of the parametric functions $\Phi_i(\xi, \eta)$ with respect to the computational coordinates (ε, ϱ). We need the same transformation defined by (4.3). Then we can write (5.1) as

$$g_{11} = \left[\sum_{i=1}^{n} x_i \left(\bar{J}_{11}\frac{\partial \Phi_i}{\partial \xi} + \bar{J}_{12}\frac{\partial \Phi_i}{\partial \eta} \right) \right]^2 + \left[\sum_{i=1}^{n} y_i \left(\bar{J}_{11}\frac{\partial \Phi_i}{\partial \xi} + \bar{J}_{12}\frac{\partial \Phi_i}{\partial \eta} \right) \right]^2$$
$$g_{22} = \left[\sum_{i=1}^{n} x_i \left(\bar{J}_{21}\frac{\partial \Phi_i}{\partial \xi} + \bar{J}_{22}\frac{\partial \Phi_i}{\partial \eta} \right) \right]^2 + \left[\sum_{i=1}^{n} y_i \left(\bar{J}_{21}\frac{\partial \Phi_i}{\partial \xi} + \bar{J}_{22}\frac{\partial \Phi_i}{\partial \eta} \right) \right]^2. \tag{5.2}$$

VI. NUMERICAL CONSIDERATIONS

Observation of (4.5) together with (5.2) shows that the matrix system to be solved for the generation of the coordinate system (x, y) is nonlinear. An iterative procedure is then required to solve system (4.5). However, there is an initial difficulty. Equation (5.2) cannot be evaluated at the first iteration, since only the (x, y) coordinates of the contour of the physical domain are known. The coordinates in the interior of the physical domain are the solution of (5.2) at this very first iteration. Then the process followed in this work is

a • Define boundary points of the physical domain

b • Solve the following elliptic system using Dirichlet boundary conditions [4]

$$\frac{\partial^2 f}{\partial \varepsilon^2} + \frac{\partial^2 f}{\partial \varrho^2} = 0 \tag{6.1}$$

which in a Bubnov–Galerkin formulation gives

$$\int_{-1}^{+1}\int_{-1}^{+1}\sum_{j=1}^{8} f_j \left\{ \left[\bar{J}_{11}\frac{\partial \Phi_j}{\partial \xi} + \bar{J}_{12}\frac{\partial \Phi_j}{\partial \eta} \right] \left[\bar{J}_{11}\frac{\partial \Phi_i}{\partial \xi} + \bar{J}_{12}\frac{\partial \Phi_i}{\partial \eta} \right] + \left[\bar{J}_{21}\frac{\partial \Phi_j}{\partial \xi} + \bar{J}_{22}\frac{\partial \Phi_j}{\partial \eta} \right] \times \left[\bar{J}_{21}\frac{\partial \Phi_i}{\partial \xi} + \bar{J}_{22}\frac{\partial \Phi_i}{\partial \eta} \right] \right\} \det[J]\, d\xi\, d\eta$$

$$= \int_{\Gamma_l} \Phi_i \frac{\partial f}{\partial \mathbf{n}}\, d\Gamma_l. \tag{6.2}$$

Dirichlet boundary conditions for (6.2) are defined using various functions for $f = f(\xi, \eta)$ at the boundary. These functions are described in the following section.

c • With calculated f values from step b solve system (4.5) using specified boundary conditions. At this stage, this is done using Cholesky's method.

d • With newly calculated x and y values, recalculate new f values using (5.2).

e • Recalculate x and y and go back to step d until convergence is obtained.

The number of iteration cycles required for convergence is the number of times the program requires to loop through steps d to e. The convergence criteria utilized in [6] has been adopted here solely for comparison purposes. This convergence criteria was specified by an index termed $\mathrm{MDO} = |\frac{1}{2}\pi - \theta|$ that measured the *localized* maximum deviation from orthogonality. Convergence was obtained when *MDO at a fixed point* stabilized within one decimal point to a constant value. The angle θ is calculated as [5]

$$\cos\theta = \frac{g_{12}}{\sqrt{g_{11}\, g_{22}}}$$

or

$$\cos\theta = \frac{T_1 T_2 + T_3 T_4}{(T_1^2 + T_3^2)^{1/2}(T_2^2 + T_4^2)^{1/2}}, \tag{6.3}$$

where

$$T_1 = \sum_{j=1}^{n} x_j \left[\bar{J}_{11} \frac{\partial \Phi_j}{\partial \xi} + \bar{J}_{12} \frac{\partial \Phi_j}{\partial \eta} \right]$$

$$T_2 = \sum_{j=1}^{n} x_j \left[\bar{J}_{21} \frac{\partial \Phi_j}{\partial \xi} + \bar{J}_{22} \frac{\partial \Phi_j}{\partial \eta} \right]$$

$$T_3 = \sum_{j=1}^{n} y_j \left[\bar{J}_{11} \frac{\partial \Phi_j}{\partial \xi} + \bar{J}_{12} \frac{\partial \Phi_j}{\partial \eta} \right]$$

$$T_2 = \sum_{j=1}^{n} y_j \left[\bar{J}_{21} \frac{\partial \Phi_j}{\partial \xi} + \bar{J}_{22} \frac{\partial \Phi_j}{\partial \eta} \right].$$

A more general convergence index could be the average deviation from orthogonality (ADO). This value would give the grid's *overall* deviation from orthogonality, since it takes into account all the corners of each element. It is defined as

$$\text{ADO} = \frac{1}{4N} \left[\sum_{k=1}^{N} \sum_{i=1}^{4} \theta_k^i \right],$$

where the subindex k refers to the element number and the superindex i refers to the element's corner, N being the number of elements. The index ADO was not used as a convergence criteria. However, values of ADO are presented together with those of MDO to give a *global* idea of the orthogonality characteristics of the whole grid.

The following section is dedicated to the results obtained for particular geometries of a physical domain, those used in [6], using the methodology presented here. We now briefly mention the types of functions used to define the shape factor f on the contour to be used in step b to solve (6.2). This definition will be codified by the parameter *ISHA* (*ISHA* = 1, 2, 3 are taken from [6]), as follows

ISHA = 0. Finite element definition of f.

ISHA = 1. Uniform shape factor distribution.

ISHA = 2. Exponential shape factor distribution.

ISHA = 3. Linear shape factor distribution.

ISHA = 4. Normal shape factor distribution given by the probability density function

$$f(\varepsilon_i) = \frac{1}{2\pi\sigma_0} e^{[-0.5(\varepsilon_i/\sigma_0)^2]}$$

σ_0 = a constant.

TABLE I

Case A. Complete Boundary Correspondence Exponential Boundary Point Distribution on the Upper Side Linear Isoparametric Elements

	MDO–ADO–Number of Iterations				
Case	$H = 0.05$	$H = 0.10$	$H = 0.15$	$H = 0.20$	$H = 0.25$
ISHA = 0	3.6–0.9–19	4.9–1.2–20	6.3–1.7–20	8.3–1.9–21	9.6–2.9–20
ISHA = 1	1.7–0.6–6	3.3–1.1–6	4.9–1.5–6	6.9–1.7–6	6.9–2.1–9
ISHA = 2	1.8–0.6–10	3.4–1.0–10	5.1–1.5–10	8.9–1.6–12	9.4–2.7–16
ISHA = 3	1.6–0.6–8	3.1–1.1–8	4.8–1.4–7	8.0–1.6–12	10.7–2.6–12
ISHA = 4	1.7–0.6–6	3.0–1.1–7	4.3–1.4–7	5.2–1.4–7	6.8–2.0–7

VI.1. Numerical Results

This section presents results obtained using the geometries and boundary conditions specified in [6] as cases *A*, *B*, and *C*. For detailed information, the reader is encouraged to refer to this reference. All results presented here are for single precision computations.

VI.1.1. *Case A. Complete Boundary Correspondence*

It was reported in [6] that *no satisfactory orthogonal grid* could be obtained using complete boundary correspondence when solving system (4.5). The cause was attributed to the asymmetry of the physical domain with the ensuing suggestion that complete boundary correspondence could only be used for symmetric regions. The method presented in this work shows otherwise. Table I shows results for the asymmetric region shown in Fig. 1. Equidistant boundary point distribution in all sides has been used, except the upper one where exponential boundary point distribution has been applied. The first quantity in each

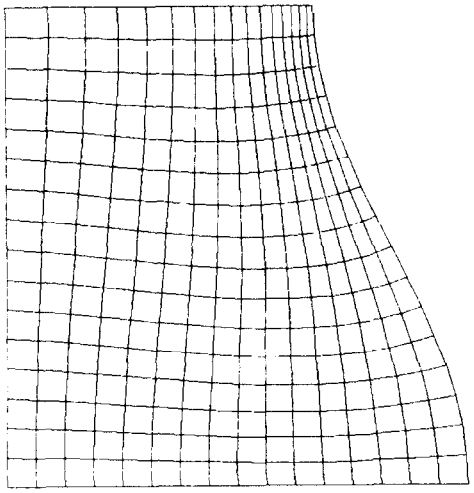

FIG. 1. 16 × 16 grid, $H = 0.15$, *ISHA* = 4. Exponential distribution of points on upper boundary.

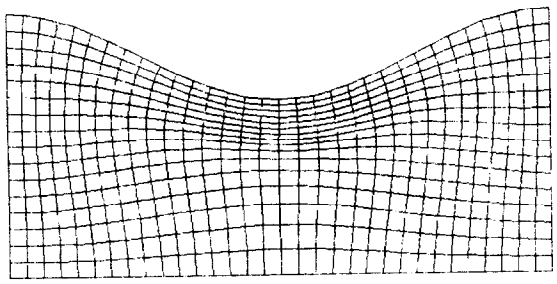

FIG. 2. 32×16 grid, $H = 0.15$, $ISHA = 3$. Equidistant distribution of points in all boundaries.

column refers to MDO, the second to ADO, and the third to the number of iterations required to attain convergence. This format of presenting *tabled* information will be used throughout this work unless otherwise stated.

It can be seen from Table I that good localized (MDO) and overall (ADO) accuracy can be obtained using complete boundary correspondence in a non-symmetric domain. Overall best values are obtained using a normal distribution for f. However, the difference in MDO for each H (H being the height of the wave-like boundary) did not show, in general, a difference greater than 3° among the five initial shape factor distributions. The corresponding difference in ADO was not greater than 0.9°. Assuming that the effect of these differences on a subsequent engineering computation is not to be very significant, the method seems to yield acceptable orthogonal grids regardless of the initial shape factor distribution. Solutions in [6] were reported as strongly dependent on such distributions. The number of iterations required to attain convergence was lowest for $ISHA = 1$ and $ISHA = 4$, i.e., constant and normal initial distribution of the shape factor. Therefore, from a CPU time point of view these initial distributions seem to be more advisable. For $ISHA = 0$, 1, and 4 the number of iterations required for MDO to be reached showed to be almost independent of H. For $ISHA = 2$ and $ISHA = 3$, a slightly higher number of iterations is required for $H = 0.2$ and $H = 0.25$.

Figure 1 shows an orthogonal grid using complete boundary correspondence for a 16×16 grid with $H = 0.15$, $ISHA = 4$. For this case, MDO was 4.3 and ADO was 1.4.

TABLE II

Case A. Complete Boundary Correspondence Exponential Boundary Point Distribution on the Upper Sde Linear Isoparametric Elements

	MDO–ADO–Number of Iterations		
Case	$H = 0.3$	$H = 0.4$	$H = 0.5$
$ISHA = 4$	12.8–6.1–5	14.6–5.8–7	22.7–11.8–4

TABLE III

Case A. Complete Boundary Correspondence Equidistant Boundary Point Distribution Linear Isoparametric Elements

	MDO–ADO–Number of Iterations				
Case	$H = 0.05$	$H = 0.10$	$H = 0.15$	$H = 0.20$	$H = 0.25$
$ISHA = 0$	6.2–2.5–17	11.1–4.7–16	16.2–6.2–16	20.4– 7.2–17	24.5– 8.2–20
$ISHA = 1$	4.2–2.8–6	8.6–5.6–6	13.1–8.1–7	17.5–10.5–11	21.6–12.6–12
$ISHA = 2$	4.2–2.8–5	8.5–5.6–11	12.9–8.1–15	17.2–10.5–13	21.2–12.6–13
$ISHA = 3$	4.6–2.8–8	9.2–5.6–7	14.1–8.1–11	18.5–10.8–14	23.1–12.6–15
$ISHA = 4$	4.4–2.8–6	8.3–5.6–7	12.6–8.1–10	16.9–10.5 13	20.9 12.6–14

A similar level of accuracy was obtained for a symmetric region with equidistant boundary correspondence in a 32×16 grid with $ISHA = 3$ and $H = 0.15$. For this case, Fig. 2, MDO was 4.2 and ADO was 1.1.

Greater values of H were used for ISHA = 4 in order to verify if the method would still converge for very large H values. Table II shows results for this case. Convergence as well as good overall orthogonality characteristics are obtained. The localized orthogonality is seen to deteriorate as H becomes extremely large.

Results for MDO and ADO are shown in Table III for equidistant boundary point distribution for the domain shown in Fig. 1. Values of MDO and ADO are roughly 2 and 4 times higher than those for exponential boundary point distribution. However, very good convergence characteristics are kept with the number of iterations again being lowest for $ISHA = 1$ and, in general, $ISHA = 4$.

It should be noted that results of Table III correspond to only three iterations. The reasoning behind stopping at iteration 3 is shown in Fig. 3. This figure shows typical con-

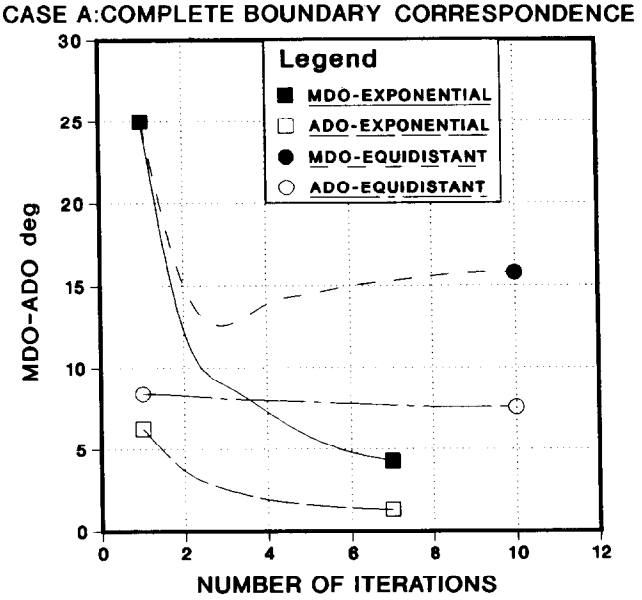

FIG. 3. Convergence characteristics for exponential and equidistant distribution of points.

TABLE IV

Case B. Dirichlet and Neuman Boundary Conditions Neuman Boundary Condition on the Upper Side Linear Isoparametric Elements

	MDO–ADO–Number of Iterations				
Case	$H=0.05$	$H=0.10$	$H=0.15$	$H=0.20$	$H=0.25$
$ISHA=0$	12.2–3.7–9	10.8–3.3–10	10.6–3.1–11	11.1–3.3–11	12.1–2.9–8
$ISHA=1$	1.6–0.6–10	3.1–0.9–13	4.6–1.2–13	5.9–1.6–14	6.8–2.3–16
$ISHA=2$	1.5–0.5–15	2.9–0.8–15	4.3–1.0–15	5.6–1.5–15	8.5–2.5–15
$ISHA=3$	1.4–0.4–10	2.7–0.7–12	4.5–1.1–14	5.1–1.3–10	7.7–2.9–7
$ISHA=4$	1.3–0.3–10	3.0–0.8–13	4.3–1.1–14	5.2–1.4–10	6.7–2.1–13

vergence characteristics for MDO and ADO as a function of the number of iterations. Although ADO has a consistently decreasing tendency, this is not the case for MDO. The index MDO tended to show a minimum at the third iteration but stabilization was achieved at a later iteration value. A very high rate of convergence in the initial few iterations was observed throughout this study. This is particularly important for subsequent computations in which orthogonality is not strictly required. Then a satisfactory global level of orthogonality could be obtained to improve results after very few cycles (normally not more than one).

VI.1.2. *Case B. Dirichlet and Neuman Boundary Conditions*

In this part, equidistant boundary correspondence is applied to all boundaries but the upper side where Neuman boundary conditions are applied. The same non-symmetric geometry as in Case A is studied. Table IV shows the results of MDO and ADO for this case.

Values of MDO for $ISHA=3$ are slightly higher than those reported in [6], the difference roughly ranging from 0.2° to 0.8°. A similar difference with $ISHA=2$ for $H\leqslant 0.15$.

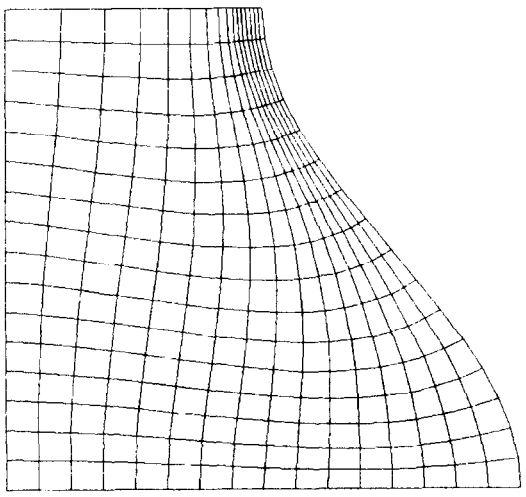

FIG. 4. 16×16 grid, $H=0.25$, $ISHA=2$. Neuman boundary condition on upper boundary.

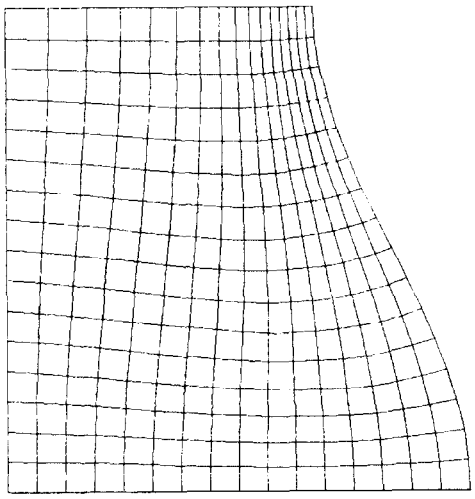

FIG. 5. 16×16 grid, $H=0.15$, $ISHA=1$. Neuman boundary condition on upper boundary.

However, for larger values of H, i.e., very steep wave forms, improved orthogonality characteristics are obtained specially for $H=0.25$ where [6] failed to converge. This last case is shown in Fig. 4. Also for $ISHA=1$, the linear shape factor distribution, it was reported in [6] that orthogonal grids could not be obtained. This is not the case in this work and Fig. 5 shows results for a 16×16 grid, $H=0.15$, $ISHA=1$. For this case, we are able to attain very good localized and overall orthogonality characteristics. It can be concluded here that the present method gives very good orthogonality characteristics regardless of the initial shape factor distribution. Convergence is also observed for all H

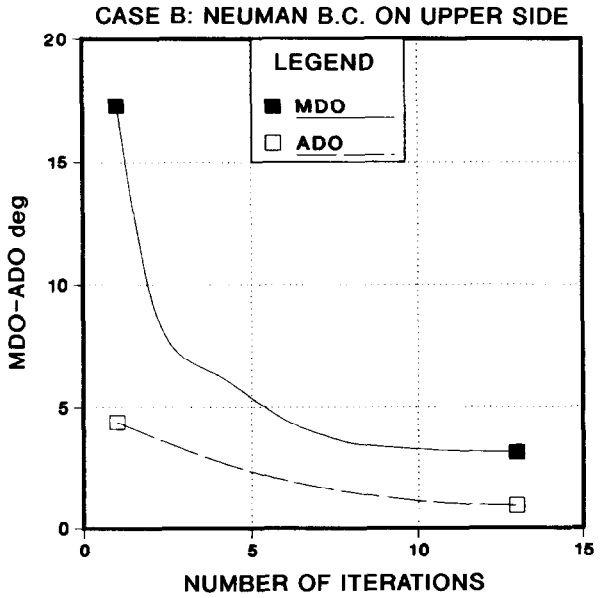

FIG. 6. Convergence characteristics for Fig. 5.

TABLE V

Case C. Dirichlet and Neuman Boundary Conditions Distribution of Boundary Conditions as Defined in [6] Linear Isoparametric Elements

	MDO–ADO–Number of Iterations				
Mesh size	$ISHA = 0$	$ISHA = 1$	$ISHA = 2$	$ISHA = 3$	$ISHA = 4$
8 × 8	6.7–2.2–8	6.6–1.5–6	6.6–1.5–12	10.2–2.2–6	7.6–1.5–6
16 × 16	4.6–1.4–9	5.9–0.7–7	4.9–0.8–6	7.0–1.1–9	6.0–0.7–9
24 × 24	3.9–1.0–11	4.6–0.5–7	3.7–0.6–6	4.5–0.8–16	4.6–0.5–8
36 × 36	3.7–0.8–10	3.8–0.4–8	2.9–0.4–6	5.6–0.6–8	3.9–0.4–8
40 × 40	2.9–0.6–10	3.2–0.3–8	2.6–0.3–6	3.6–0.5–19	3.4–0.3–7
48 × 48	2.3–0.5–10	2.8–0.2–8	2.3–0.3–6	4.4–0.4–9	2.9–0.2–6

values and shape factors used. The number of iterations is again, in general, only slightly affected as H increases.

For the case shown in Fig. 5, convergence rates for MDO and ADO as a function of the number of iterations are shown in Fig. 6. In the presence of Neuman boundary conditions both MDO and ADO exhibited a decreasing tendency until convergence was obtained. The rate of convergence, however, seems to be slower than that for Case A using exponential boundary point distribution for a similar level of accuracy.

VI.1.3. *Case C. Combination of Neuman and Dirichlet Boundary Conditions*

In this case, a combination of Dirichlet and Neuman boundary conditions is used as specified in Table I of [6]. Results for 4- and 8-noded isoparametric elements are presented. Some CPU time values are also given. These were obtained using an IBM 3081K.

Table V shows the results of MDO and ADO for the geometry of Fig. 1 as a function of the number of elements and *ISHA* for linear elements. These can be readily compared with those of Table IV in [6].

Values of the MDO here are consistently higher than those reported in [6], the difference ranging in general from 1.5 to 5.0°. Values of ADO are very low, securing excellent

TABLE VI

Case C. Dirichlet and Neuman Boundary Conditions Distribution of Boundary Conditions as Defined in [6] Quadratic Isoparametric Elements

	MDO–ADO–Number of Iterations				
Mesh size	$ISHA = 0$	$ISHA = 1$	$ISHA = 2$	$ISHA = 3$	$ISHA = 4$
8 × 8	6.3–1.8–19	4.3–1.0–13	3.7–0.8–9	3.3–0.5–4	3.3–0.5–5
16 × 16	4.9–1.9–7	2.3–0.4–6	1.4–0.2–5	1.9–0.4–19	3.9–0.5–5
24 × 24	3.3–0.6–9	2.0–0.3–6	1.9–0.3–4	1.8–0.3–17	4.8–0.4–3
36 × 36	2.9–0.4–11	1.7–0.3–6	1.9–0.3–4	2.8–0.4–11	2.9–0.4–11
40 × 40	2.7–0.3–11	1.4–0.3–6	2.0–0.3–4	4.3–0.3–5	4.6–0.3–5
48 × 48	3.4–0.4–8	1.6–0.2–6	2.2–0.3–4	1.7–0.2–8	1.0–0.1–8

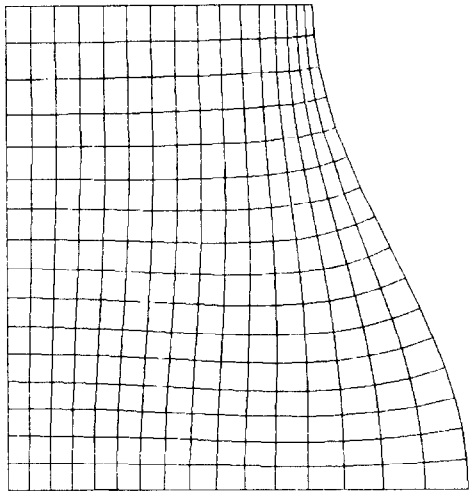

FIG. 7. 16 × 16 grid, $H = 0.15$, $ISHA = 2$. Linear isoparametric elements.

overall orthogonality, which was observed to be very close to 90° in most points of the grids. It can be seen that the MDO parameter shows very little improvement, if any, over those given in Tables I and IV, i.e., Cases A and B. In other words, localized orthogonality is not improved by increasing the use of Neuman boundary conditions. However, significant improvement in the overall orthogonality characteristics (ADO) is observed over results shown in Table I, in some cases the improvement being 50%. Although $ISHA = 0$ gave the poorest results in Case B, some of the best results are obtained here with this particular initial shape function distribution. A more noticeable improvement in MDO is also realized as N increases.

Table VI shows results for the same conditions as Table V for quadratic elements. In this case, overall

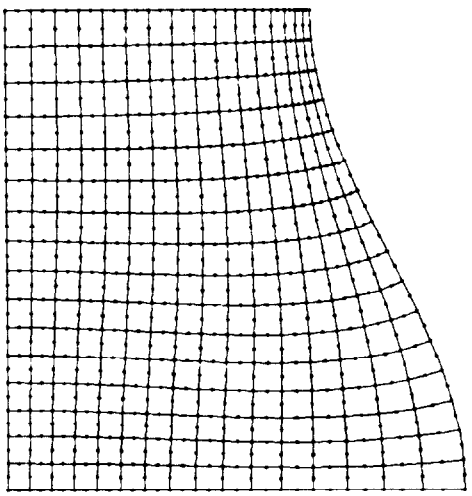

FIG. 8. 16 × 16 grid, $H = 0.15$, $ISHA = 2$. Quadratic isoparametric elements.

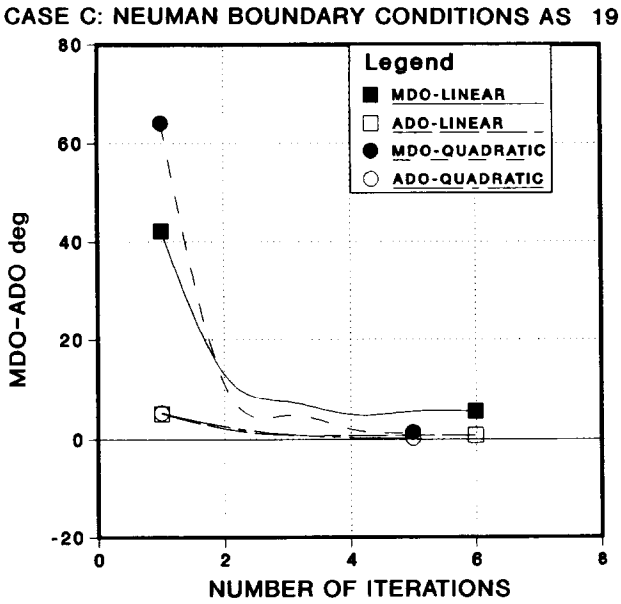

FIG. 9. Convergence characteristics for Figs. 7 and 8.

improved results are obtained for both MDO and ADO. For the latter the improvement was very significant with reductions exceeding 50%. Figures 7 and 8 show typical results for 16×16 grid using linear and quadratic elements, respectively. The position of the mid-side nodes for quadratic elements is shown in Fig. 8.

A slight reduction in the number of iterations to attain convergence is evident from the comparison of Tables V and VI, suggesting a higher rate of convergence for quadratic elements. Convergence rates corresponding to Figs. 7 and 8 are shown in Fig. 9. The higher rate of convergence exhibited by quadratic elements is apparent from this figure.

The reduction in the number of iterations of the quadratic elements did not preclude the CPU time from being significantly higher than in the case of linear elements. CPU time values corresponding to Table V are given in Table VII. The experience gathered in this work leads us to recommend the use of linear elements for grid generation. If however, quadratic elements are used for subsequent computations, it is highly advisable to devise an interpolation procedure (possibly splines) to locate the mid-side nodes of the finite element rather than mapping the entire 8-noded element.

TABLE VII

Case C. Dirichlet and Neuman Boundary Conditions Distribution of Boundary Conditions as Defined in [6] Linear Isoparametric Elements

CPU Time Required for Convergence of Results of Table V

Mesh size	$ISHA = 0$	$ISHA = 1$	$ISHA = 2$	$ISHA = 3$	$ISHA = 4$
8×8	1.7	1.3	2.3	1.3	1.4
16×16	8.6	6.9	5.2	11.2	8.6
24×24	30.5	20.2	17.6	43.3	22.8
36×36	65.5	55.4	41.8	53.4	53.4
40×40	133.4	108.5	83.5	245.1	95.9
48×48	244.7	199.2	153.0	221.6	152.9

CONCLUSIONS

A Bubnov–Galerkin procedure has been used to solve the elliptic generation system developed in [4] for constructing boundary-fitted curvilinear orthogonal coordinates. Numerical aspects have been studied using the geometries presented in [6] with some shape factor distributions proposed in [6] and some proposed here. A number of improvements have been obtained and essentially different conclusions have been realized.

Orthogonal grids of very good overall/global accuracy for both Dirichlet and Neuman boundary conditions in symmetric and asymmetric regions were obtained. Localized accuracy is lowest for the case of equidistant boundary correspondence in an asymmetric domain. For all other boundary conditions, including complete boundary correspondence with exponential boundary point distribution on one side of the domain, localized accuracy is very good in both symmetric and asymmetric domains.

The scheme showed to be stable for all degrees of asymmetry and shape factor distributions used here. Convergence was observed to be independent of these considerations. The number of iterations required for convergence was in general quite low, indicating the fast convergence characteristics of the scheme. In most cases, independence of the number of iterations on the shape factor distribution was observed.

Results obtained with linear and quadratic elements suggest that, although the latter are superior in accuracy, the former are highly preferable from CPU time considerations. For computational applications where quadratic elements are to be used, it is recommended that an interpolation scheme be devised from the mesh generated with linear/4-noded elements to locate the mid-side nodes of the 8-noded element.

The method presented in [4] is therefore considered highly reliable when solved using a Bubnov–Galerkin formulation.

REFERENCES

1. B. A. Finlayson, *The Method of Weighted Residuals* (Academic Press, New York/London, 1972).
2. J. F. Thompson, Z. U. A. Warsi, and W. C. Mastin, *Numerical Grid Generation, Foundations and Applications* (Elsevier Science, New York, 1985).

3. J. F. Thompson, *AIAA J.* **22**, 1505 (1985).
4. G. Ryskin and L. G. Leal, *J. Comput. Phys.* **50**, 71 (1983).
5. L. P. Eisenhart, *An Introduction to Differential Geometry With Use of Tensor Calculus* (Princeton Univ. Press, Princeton, NJ, 1940).
6. E. D. Chikliwala and Y. C. Yortsos, *J. Comput. Phys.* **57**, 391 (1985).
7. I. G. Bubnov, in *Symp. Inst. Commun. Eng., No. 81.* All Union Special Planning Office, 1913. See S. G. Mikhlin, *Variational Methods in Mathematical Physics* (Macmillan Co., New York, 1964).
8. B. G. Galerkin, *Vestn. Inzh. Tech.* **19**, 897 (1915) [Russian]; translation 63-18924, Clearinghouse, *Fed. Sci. Tech. Info.*, Springfield, VA, 1963.
9. C. E. Springer, *Tensor and Vector Analysis With Applications To Differential Geometry* (Ronald Press, New York, 1962).
10. O. C. Zienkiewicz, *The Finite Element Method In Engineering Science* (McCraw–Hill, New York, 1977).
11. T. J. Chung, *Finite Element Analysis in Fluid Dynamics* (McGraw–Hill, New York, 1978).
12. I. Babuska, *Computing* **6**, 264 (1970).